Recovery times of riparian vegetation

AGU PUBLICATIONS

Water Resources Research

RESEARCH ARTICLE

10.1002/2015WR018490

Recovery times of riparian vegetation

R. Vesipa[1], C. Camporeale[1], and L. Ridolfi[1]

[1]Department of Environment, Land and Infrastructure Engineering, Politecnico di Torino, Torino, Italy

Key Points:
- River flow fluctuations strongly impact the riparian vegetation recovery times
- The analytical expression of the plot-dependent mean recovery time is obtained
- The impact of man-induced hydrological alterations is discussed

Correspondence to:
R. Vesipa,
riccardo.vesipa@polito.it

Citation:
Vesipa, R., C. Camporeale, and L. Ridolfi (2016), Recovery times of riparian vegetation, *Water Resour. Res.*, *52*, doi:10.1002/2015WR018490.

Received 11 DEC 2015
Accepted 18 MAR 2016
Accepted article online 21 MAR 2016

Abstract Riparian vegetation is a key element in a number of processes that determine the ecogeomorphological features of the river landscape. Depending on the river water stage fluctuations, vegetation biomass randomly switches between growth and degradation phases and exhibits relevant temporal variations. A full understanding of vegetation dynamics is therefore only possible if the hydrological stochastic forcing is considered. In this vein, we focus on the recovery time of vegetation, namely the typical time taken by vegetation to recover a well-developed state starting from a low biomass value (induced, for instance, by an intense flood). The analytical expression of the plot-dependent recovery time is given, the role of hydrological and biological parameters is discussed, and the impact of river-induced randomness is highlighted. Finally, the effect of man-induced hydrological changes (e.g., river damming or climate changes) is explored.

1. Introduction

The riparian zone is an extremely biodiverse transitional environment, that separates freshwater bodies from the upland communities. It is a fragile ecotone that behaves as a critical zone [in the sense of *Gurnell et al.*, 2015], and it is highly affected by the fluctuations of the river stage [*Naiman et al.*, 2005]. The riparian zone has an important environmental and ecological significance. It catalyzes key ecomorphological processes and is the habitat of a great variety of fauna and flora [*Malanson*, 1993]. Riparian wetlands also protect the bankline from erosion and collapse [*Docker and Hubble*, 2008]. Furthermore, the alternation between wet and dry conditions is essential for a number of biochemical reactions that decrease the availability of nutrients and the toxicity of contaminants, providing rivers the capability of nitrogen removal [*Craig et al.*, 2008].

The riparian vegetation is the plant community that develops near rivers and is a key component of the riparian ecotone. It is highly influenced by variations of the groundwater table and by the occurrence of floodings [*Tockner et al.*, 2000]. Over the last decade, a fruitful research activity has shown that riparian vegetation plays a fundamental biogeomorphological role in setting the geomorphic units of the river morphology [*Camporeale et al.*, 2013]. It can actively modify the river landscape, by interacting with sediment transport. In past geological eras, riparian vegetation induced morphological upheavals at the planetary scale [*Gibling and Davies*, 2012]. During the Paleozoic, riparian plants colonized the banks of ancient rivers for the first time. This caused a widespread braiding-meandering transition, that, in turn, allowed the development of a great number of novel animal and vegetal species [*Gibling and Davies*, 2012].

A feature of riparian vegetation dynamics is that the plant biomass fluctuates both in time and space, as a result of river stage oscillations. A largely investigated example is given by the riparian vegetation of Tagliamento River. It flows in the north-east Italy and is still in almost pristine conditions [*Ward et al.*, 1999]. The vegetation cover undergoes very fast dynamics, where phases of strong degradation are followed by phases of recover. Vegetation biomass can be significantly reduced by floods with recurrence interval as small as 2 years [*Surian et al.*, 2015]. As a result, the age composition of the population is low: 50% (90%) of plants are younger than 10 (23) years.

In this context of high biomass reshaping, the vegetation recovery time is an important element for maintaining a well vegetated river. It is the time that vegetation spends to recover from a low value of biomass to a higher value. Several field studies [*Beschta and Ripple*, 2006; *Marshall et al.*, 2013] have shown that understanding how the recovery of biomass is related to the hydrological and biological characteristics is a key point.

In this framework, the case of vegetation dynamics occurring in the Yellowstone Park is emblematic. As a result of wolves suppression in 1920, elk population overgrew. Excessive browsing by elks on shrubs caused the decline of the population of willow. As willows are an essential food and dam building materials for beavers, the decline of the whole beaver population followed soon after [*Singer et al*., 1994]. Reintroduction of wolves in 1995 caused the elk population to fall [*Beschta and Ripple*, 2006], but with little effect in recovering the former riparian asset [*Marshall et al*., 2013]. In fact, without the ponds induced by beaver dams, the hydrological condition (position of the phreatic surface) do not allow for the recovery of the willow communities, and, in turn, for the beavers restocking. Other cases concern the recovery of riparian vegetation after wildfires [*Smith et al*., 2009] or clear cutting [*Blanchard and Holmes*, 2008; *Kurokochi et al*., 2010]. The slow recovery of vegetation after a strong destruction can open the way to transitions from indigenous vegetation to exotic species [*Smith et al*., 2009; *Kurokochi et al*., 2010]. Finally, from a more theoretical standpoint, the assessment of the recovery dynamics is fundamental for understanding the resilience of ecological systems forced by stochastic components [*Srinivasan and Kumar*, 2015].

Over the last years, several theoretical and experimental studies have considered riparian vegetation dynamics. It was demonstrated that changes in the probabilistic structure of river water stages (by dam regulations or climate changes) may induce catastrophic damage on the vegetation. Examples are the reduction of biomass and the switching of the dominant species [*Shafroth et al*., 2002; *Tealdi et al*., 2011; *Doulatyari et al*., 2014]. Other works [*Camporeale and Ridolfi*, 2006; *Muneepeerakul et al*., 2007] modeled the key role of stochasticity in generating complex behaviors in the spatiotemporal dynamics of vegetation on nonevolving topography, such as noise-induced stability and bimodality [*Camporeale and Ridolfi*, 2007]. The geomorphological changes induced by vegetation have also attracted a great deal of interest [*Wu et al*., 2005; *Crosato and Saleh*, 2011; *Nicholas et al*., 2013; *Bertoldi et al*., 2014; *Crouzy et al*., 2015]. Very recently, the interactions between vegetation and topography have also been explored [*Vesipa et al*., 2015]. Nevertheless, the recovery dynamics of riparian vegetation have never been modeled. The aim of this paper is to fill this gap.

We will adopt the minimalistic approach that has been successfully used over the last years to understand a number of ecomorphological processes [*Camporeale et al*., 2013]. The purpose of this approach is to obtain realistic and, at the same time, simple stochastic models that can describe the essential physical and the biological processes, while preserving the analytical solvability [*Camporeale et al*., 2013]. In this way, computationally demanding numerical simulations can be avoided. Moreover, the key role of noise is explicitly embedded in the mathematical framework. Therefore, this approach is particularly suitable for the comprehension of the role of flow randomness in riparian ecomorphodynamics.

2. Theoretical Framework

2.1. Key Features

A typical riparian transect is sketched in Figure 1a. Riparian vegetation lives on the bank and its evolution depends on the river stage, h^*, and on the depth of the phreatic surface, δ^* (the star denotes a dimensional quantity). As riparian soil permeability is usually high, the groundwater table position can be assumed equal to the stream stage.

For any stage h^*, both inundated and exposed zones occur in the transect. In the submerged zone (zone I in Figure 1a), vegetation suffers from flow-induced physical damage [*Yanosky*, 1980], anoxia [*Kozlowski*, 1984], burial [*Hupp*, 1988], uprooting and sediment removal [*Osterkamp and Costa*, 1987]. As a result, the plot biomass reduces with a degradation rate dependent on the local water depth. In fact, several mechanisms responsible of biomass degradation (e.g., physical damage and uprooting) are controlled by the stream-induced shear stresses, which are proportional to the water depth.

When the plot is exposed (zones II–IV in Figure 1a), the (phreatophyte) vegetation biomass dynamics depend on the depth of the groundwater table, δ^* [*Camporeale and Ridolfi*, 2006; *Tron et al*., 2015]. If δ^* falls in the species-specific range $[\delta_1^*, \delta_2^*]$ plants can uptake water and grow (zone III). When $\delta^* < \delta_1^*$ (or $\delta^* > \delta_2^*$) the root anoxia (or the weak capillary fringe) makes the water uptake difficult (zones II and IV). The boundaries of this range read $\delta_{1,2}^* = \delta_{opt}^* \mp \sqrt{1/a}$, where δ_{opt}^* is the phreatic surface depth that allows the optimal plant growth [*Kozlowski*, 1984; *Naumburg et al*., 2005], and a is a parameter describing the sensitivity of the vegetation to the departure of the groundwater table depth from δ_{opt}^*.

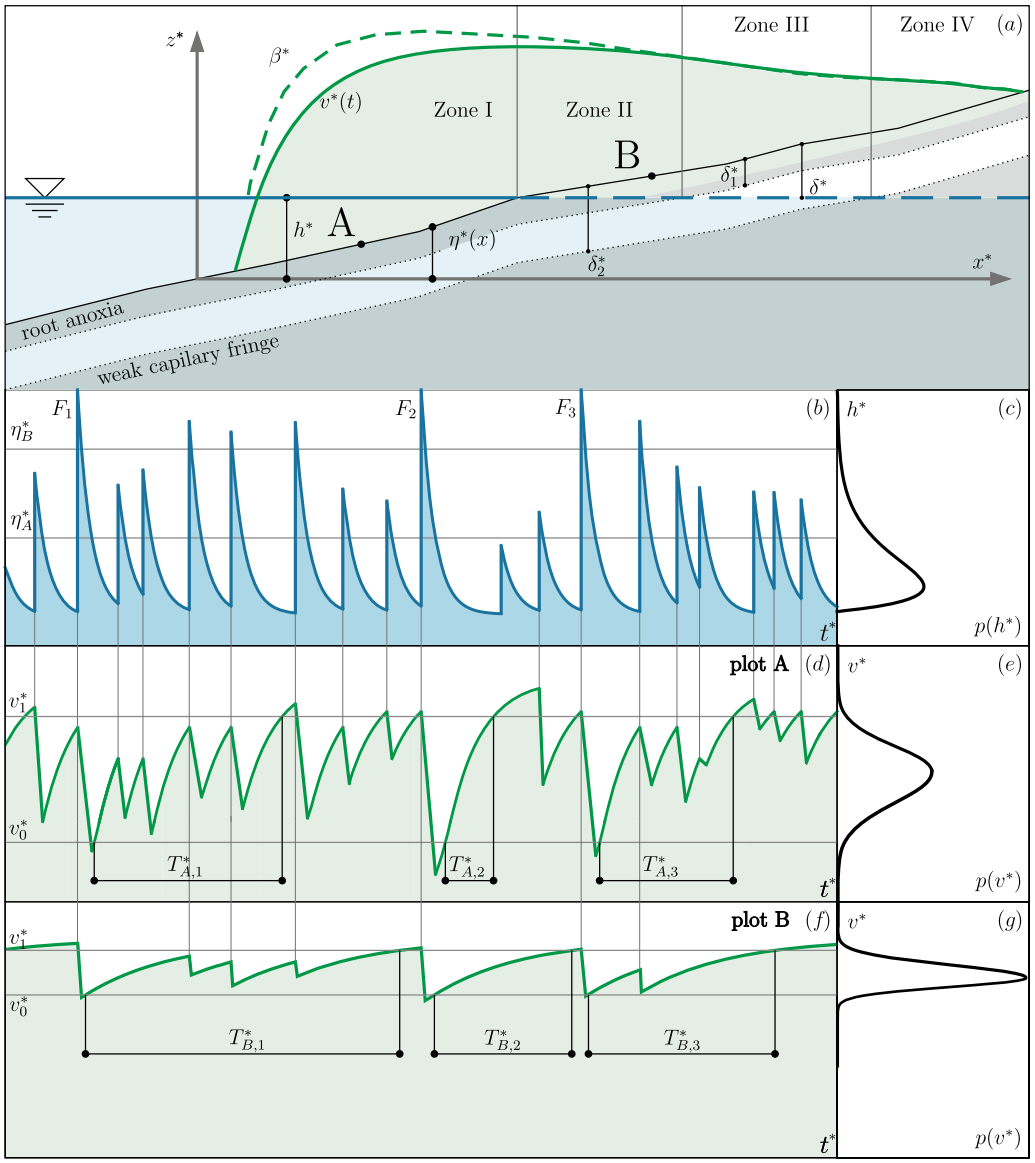

Figure 1. (a) Sketch of a riparian plot. The blue thick line marks the position of the water stage and phreatic surface. The gray areas indicate the soil regions where the phreatic surface is unsuitable for the vegetation growth in the corresponding surface plots. The white layer between gray regions marks the soil region appropriate for vegetation growth. The green dashed line gives the spatial distribution of the local mean carrying capacity, β^*, while the green continuous line gives the biomass, $v^*(t)$, at generic time t. (b, c) The (qualitative) time series and pdf of the water stage. The corresponding time series and pdf of the vegetation biomass at plot (d, e) A and (f, g) B, respectively. For sake of simplicity, (d, f) in the biomass time series, the effect of the position of the groundwater table on the vegetation growth is not reported.

Rivers exhibit random fluctuations of the water level (see Figure 1b). It follows that any plot experiences flooding and exposure periods of random duration and intensity. Therefore, both the water depth (during inundations) and the phreatic surface depth (during exposure phases) are random variables. They depend (i) on the probabilistic structure of the river water stage—which is described by the correlation time, τ^*, and by the probability density function (pdf), $p(h^*)$ (see Figure 1c)—and (ii) on the topographic elevation of the plot, η^*. For instance, in Figure 1b, we highlight the different number and the different magnitude of the flooding events experienced by plots A and B, where $\eta^*(A) < \eta^*(B)$. This plot-dependent random sequence of inundation/exposure periods impacts strongly vegetation dynamics. In fact, it gives rise to plot-specific biomass time series, where growth and degradation phases randomly alternate (see Figures 1d and 1f). As a result, the vegetation biomass, v^*, exhibits a stochastic dynamics which can be conveniently described by plot-specific pdfs (Figures 1e and 1g) [*Camporeale and Ridolfi*, 2006].

Randomness is therefore a crucial component of the riparian environment, as river flow fluctuations can induce relevant biomass variations, depending on the intensity and persistence of the hydrological forcing. In this framework, a key issue concerns the time, T^*, required to vegetation to recover from low biomass values (typically induced by severe floods). The recovery time is the result of a complex interplay between biomass growth/degradation phases induced by river flow dynamics. It follows that biological, hydrological, and morphological components contribute to determine T^*.

In order to clarify this aspect, let us consider the example shown in Figure 1. Three strong flooding events, F_1, F_2, and F_3 are highlighted in Figure 1b. In plots A and B, they cause a reduction of the biomass below the value v_0^* (see Figures 1d and 1f), that is assumed as a low biomass threshold. Consider now the recovery dynamics of vegetation after these flood events. A threshold v_1^* is chosen to identify well-developed vegetation. Note that the thresholds v_0^* and v_1^* are plot dependent, in order to mirror the differences between the biomass pdfs typical of each plot. After F_1, several floods hamper v^* to reach v_1^* in short time and the recovery times $T_{A,1}^*$ and $T_{B,1}^*$ are long. After F_2, no flood halts the growth of v^* and v_1^* is reached very quickly (i.e., $T_{A,2}^*$ and $T_{B,2}^*$ are short). In the case of flood F_3, an intermediate behavior is observed.

These examples show that the recovery time of vegetation from two fixed biomass values strongly depends on the durations of flooding and exposure periods, and on the frequency and magnitude of the inundations. Hence, the quantity T^* is a stochastic variable as well, and it is plot specific. In the following, the theory of mean first passage times of noise-driven phenomena will be used to evaluate the local mean value, $\bar{T}^*$, of the recovery times.

2.2. Stochastic Modeling

In this section, the main points of the stochastic model by *Camporeale and Ridolfi* [2006] are recalled. They provide a starting point for the recovery time evaluation and readers can refer to the original work for further details. The vegetation stochastic dynamics at a generic plot of coordinate x^* (see Figure 1a) are modeled as

$$\frac{dv^*}{dt^*} = \begin{cases} -K(h^* - \eta^*)v^{*n} & h^* \geq \eta^* \quad (a) \\ \\ \alpha_2 v^{*m}(V_{cc}^* - v^*)^{*p} & h^* < \eta^* \quad (b) \end{cases} . \tag{1}$$

Equation (1a) models the degradation of vegetation biomass due to uprooting, anoxia, and burial occurring when the plot is flooded (i.e., $h^* \geq \eta^*$). The parameter K is a species-specific coefficient that quantifies the vegetation tolerance to floods, and the higher the term $(h^* - \eta^*)$ the higher the vegetation degradation. On the other hand, equation (1b) describes the vegetation growth when the plot is exposed (i.e., $h^* < \eta^*$). The term α_2 is the species-specific growth rate, while V_{cc}^* is the plot-specific carrying capacity. Model (1) is stochastic, as the degradation rate, the carrying capacity, and the switching between equations are forced by the random variable, h^*. In the following, we will set $m = n = p = 1$.

Dimensionless variables are introduced. The plot elevation, η^*, is made dimensionless as $\eta = (\eta^* - \bar{h}^*)/\bar{h}^*$, where $\bar{h}^*$ is the river mean water depth. This scaling is adopted for all the vertical lengths, so that the river free surface position, h, has null average value and $\min[h] = -1$. The biomass is normalized by the maximum carrying capacity, $v_{\max}^*$. It is the species-specific biomass that a riparian plot can sustain when the phreatic surface remains constant at the depth δ_{opt}^*. It follows that $v = [0, 1]$. With this scale, it is easy to define the dimensionless carrying capacity, namely, $V_{cc} = 1 - a(\delta - \delta_{opt})^2$ if $\delta_1 \leq \delta \leq \delta_2$ and zero otherwise, where the depth of the phreatic surface reads $\delta = \eta - h$. We finally introduce the dimensionless time $t = t^* \cdot \alpha_2$ so that (1) becomes

$$\frac{dv}{dt} = \begin{cases} -\alpha_1 v^n & h \geq \eta \quad (a) \\ \\ v^m(V_{cc} - v)^p & h < \eta, \quad (b) \end{cases} \tag{2}$$

where $\alpha_1 = k(h - \eta)$ and $k = K/\alpha_2$.

In order to solve the stochastic model (2), the average rate of vegetation degradation, α, and the mean carrying capacity, β, are introduced [*Camporeale and Ridolfi*, 2006, 2007]. They read

$$\alpha=\frac{1}{P_I}\int_{\eta}^{\infty}\alpha_1 p(h)\mathrm{d}h=\frac{1}{P_I}\int_{\eta}^{\infty}k(h-\eta)p(h)\mathrm{d}h, \tag{3}$$

$$\beta=\frac{1}{P_E}\int_{-1}^{\eta}V_{cc}p(h)\mathrm{d}h=\frac{1}{P_E}\int_{-1}^{\eta}1-a(\eta-h-\delta_{opt})^2p(h)\mathrm{d}h, \tag{4}$$

where $P_I=\int_{\eta}^{\infty}p(h)\mathrm{d}h$ and $P_E=\int_{-1}^{\eta}p(h)\mathrm{d}h$ are the probability of being in inundated or exposure conditions, respectively.

The average values, α and β, replace the functions α_1 and V_{cc} in the model (2) so that two new functions, $f_I(v)=-\alpha v$ and $f_E(v)=v(\beta-v)$, are obtained. They describe the vegetation dynamics in inundated and exposed conditions, respectively, and (2) can be expressed by the single stochastic differential equation

$$\frac{\mathrm{d}v}{\mathrm{d}t}=f(v)+\xi(t)\cdot g(v), \tag{5}$$

where $\xi(t)$ is a dichotomous Markov process that switches between the values Δ_I and Δ_E, while functions $f(v)$ and $g(v)$ read

$$f(v)=\frac{\Delta_I f_E-\Delta_E f_I}{\Delta_I-\Delta_E},\ g(v)=\frac{f_E-f_I}{\Delta_E-\Delta_I}. \tag{6}$$

The solution of (5) is the plot-specific probability density function of the vegetation biomass. It reads [*Ridolfi et al.*, 2011]

$$p(v)=N\frac{g(v)}{\Phi(v)}\exp\left[-(k_E+k_I)\int\frac{f(v')}{\Phi(v')}\mathrm{d}v'\right], \tag{7}$$

where k_E and k_I are the average switching rates of the flooded and exposure conditions at the plot, respectively, and

$$\Phi(v)=[f(v)+\Delta_I g(v)]\cdot[f(v)+\Delta_E g(v)]=\alpha v(\beta-v). \tag{8}$$

Equations (2)–(8) are valid for any pdf of the water stage, $p(h)$. A common choice [*Doulatyari et al.*, 2014; *Tron et al.*, 2015] is to model water stage time series as a random sequence of exponentially distributed jumps (i.e., a white shot noise), and exponential decays. In this case, $p(h)$ is the Gamma distribution

$$p(h)=\frac{\lambda^{\lambda}e^{-(h+1)\lambda}(h+1)^{\lambda-1}}{\Gamma[\lambda]}, \tag{9}$$

where $\lambda=1/C_h^2$ (C_h is the coefficient of variation of the water level) and $\Gamma[\cdot]$ is the Gamma function [*Abramowitz and Stegun*, 1964]. In this case, k_E can be analytically evaluated as the inverse of the mean first passage time between two flooding events [*Laio et al.*, 2001], while it can be demonstrated that $k_I=k_E P_E/P_I$. Moreover, without any loss of generality [*Kitahara et al.*, 1980; *Vandenbroeck*, 1983; *Camporeale and Ridolfi*, 2006], it can be assumed that $\Delta_E=1$ and that $\xi(t)$ has a vanishing average value, namely $\Delta_I k_E+\Delta_E k_I=0$. The calculation of α, β, k_E, and k_I is straightforward for a Gamma-distributed water stage, and the analytical expressions are given in Appendix A.

2.3. Mean Recovery Times

The mean recovery time of vegetation biomass, $\bar{T}$, is obtained by the mathematical approach developed by *Sancho* [1985] regarding the mean first passage time in dynamical systems driven by dichotomous noise (DSDN). These systems are characterized by two different deterministic dynamics that alternate (e.g., growth and decay). The switching between these dynamics is given by an external two-state random forcing (see the example shown in Figure 2). A generic DSDN is described by the single stochastic equation $\mathrm{d}y/\mathrm{d}t=f(y)+\xi(t)g(y)$, where y is the system variable and $\xi(t)$ is the dichotomous process. This latter assumes values $\Delta_1>0$ or $\Delta_2<0$ with switching rates k_1 and k_2 (see Figure 2b), and it has null average, i.e., $\Delta_1 k_2+\Delta_2 k_1=0$. Finally, functions $f(y)$ and $g(y)$ are such that $f(y)+\xi(t)g(y)$ reduces to one of the two deterministic dynamics of the DSDN, depending on the value of $\xi(t)$ [*Ridolfi et al.*, 2011].

According to *Sancho* [1985], the average time $\bar{T}(y_0,y_1)$ required to the systems to evolve from an initial state y_0 to a final threshold y_1 can be evaluated as

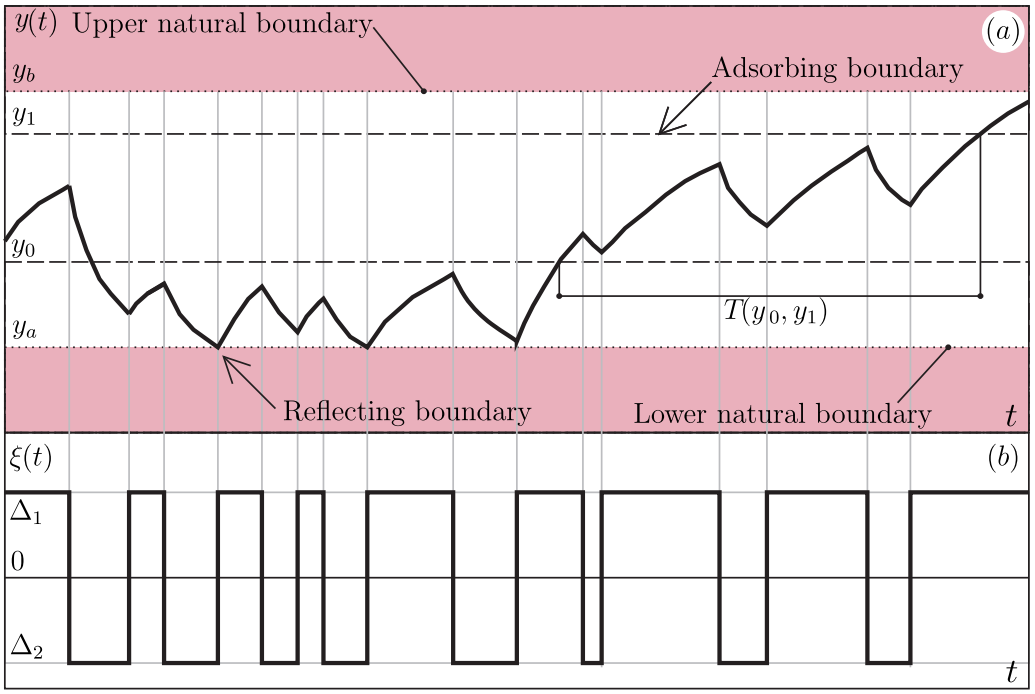

Figure 2. (a) Example of stochastic dynamics driven by dichotomous noise. y is the system variable and y_a and y_b are the natural boundaries (i.e., the system evolves in the white region). y_0 and y_1 are the starting and final states chosen to evaluate the mean passage time, $\bar{T}(y_0, y_1)$. (b) Corresponding realization of the dichotomous process $\xi(t)$.

$$\bar{T}(y_0, y_1) = (k_1 + k_2) \int_{y_0}^{y_1} \frac{\Theta(y)}{\Psi(y)\Phi(y)} \mathrm{d}y, \tag{10}$$

where

$$\Psi(y) = [f(y_b) + \Delta_1 g(y_b)]^{-1} \exp\left[\int^{y} \frac{(k_1 + k_2) f(y\prime)}{\Phi(y')} \mathrm{d}y'\right], \tag{11}$$

$$\Phi(y) = [f(y_0) + \Delta_1 g(y_0)][f(y_0) + \Delta_2 g(y_0)], \tag{12}$$

and

$$\Theta(y) = \int_{y_a}^{y} \Psi(u) \mathrm{d}u. \tag{13}$$

In the former equations, y_a and y_b are the natural boundaries of the system (see Figure 2a), namely $f(y_a) + \Delta_1 g(y_a) = 0$ and $f(y_b) + \Delta_2 g(y_b) = 0$.

Three additional conditions must be satisfied. First, $y_a \leq y_0 \leq y_1$. Second, y_a is a reflecting boundary; i.e., y cannot reduce below y_a (see Figure 2a, arrow on the bottom). Finally, y_1 is an adsorbing boundary; i.e., y can be larger than y_1 (see Figure 2a, arrow on the top). From a mathematical point of view, these conditions read

$$\left.\frac{\partial \bar{T}(y_0, y_1)}{\partial y_0}\right|_{y_a} = 0, \quad \bar{T}(y_0, y_1) = 0. \tag{14}$$

The solution by *Sancho* [1985] is here used to evaluate the mean recovery times of riparian vegetation biomass, $\bar{T}(v_0, v_1)$. To this aim, the stochastic equation (5) is used for describing the system evolution. In this case, the natural boundaries of the system are given by

$$f(v_a) + \Delta_I g(v_a) = 0, \quad f(v_b) + \Delta_E g(v_b) = 0, \tag{15}$$

namely $v_a = 0$ and $v_b = \beta$. It can be observed that (i) v cannot go below $v_a = 0$ and then v_a is a reflecting boundary and (ii) if $v_1 < \beta$, the upper threshold v_1 can be exceeded, and v_1 is an adsorbing boundary. All these properties are in the agreement with the hypotheses necessary to obtain relation (10).

It is therefore possible to use relation (10) for our problem (5), so that the recovery time of vegetation reads

$$\bar{T}(v_0, v_1) = (k_I + k_E) \int_{v_0}^{v_1} \frac{\Theta(v)}{\Psi(v)\Phi(v)} \mathrm{d}v, \tag{16}$$

where considering (11) and (12),

$$\Psi(v) = (\beta - v)^{k_E/\beta - 1} \left[v^{k_I/\alpha - (\beta + k_E)/\beta} \right], \tag{17}$$

and

$$\begin{aligned} \Theta(v) = \frac{\alpha}{\alpha k_E - \beta k_I} \cdot \Bigg\{ & (\beta - v)^{k_E/\beta} v^{k_I/\alpha - k_E/\beta} \, {}_2F_1 \left[1, \frac{k_I}{\alpha}, -\frac{k_E}{\beta} + \frac{k_I}{\alpha} + 1, \frac{v}{\beta} \right] \\ & - (\beta - v_c)^{k_E/\beta} v_c^{k_I/\alpha - k_E/\beta} \, {}_2F_1 \left[1, \frac{k_I}{\alpha}, -\frac{k_E}{\beta} + \frac{k_I}{\alpha} + 1, \frac{v_c}{\beta} \right] \Bigg\}. \end{aligned} \tag{18}$$

In the former equations, ${}_2F_1[\cdot, \cdot, \cdot, \cdot]$ is the hypergeometric function [*Abramowitz and Stegun*, 1964], while the integral in (16) can be easily evaluated numerically.

The previous relations can be used for any set of threshold values (v_0, v_1). In order to investigate typical behaviors, we set the initial value, v_0, as the fifth percentile of the biomass pdf. This value is characteristic of a flood-damaged vegetation and is relatively rare for the plot. It occurs as a result of unfavorable hydrological events that are detrimental for vegetation. Examples are (i) a single extreme flood (high water submersion) that destroys at once most of biomass or (ii) a number of weak (low water submersion) but frequent inundations that reduce biomass during many events. Moreover, we set $v_1 = \mu$, i.e., we consider the mean value of $p(v)$ as representative of a well-developed vegetation (for the specific site). As these thresholds depend on the vegetation pdf, they are plot specific.

In order to highlight the key role played by random disturbances induced by river stage fluctuations, we consider also the hypothetical situation in which no flooding periods occur in the plot (i.e., vegetation biomass never reduces). In this case, the time required to vegetation for recovering from v_0 to v_1 can be simply evaluated by the deterministic equation (2b). This recovery time in undisturbed conditions reads

$$\hat{T}(v_0, v_1) = \int_{v_0}^{v_1} \frac{\mathrm{d}v}{v(1-\beta)}. \tag{19}$$

The metric

$$r(v_0, v_1) = \frac{\bar{T}(v_0, v_1)}{\hat{T}(v_0, v_1)} - 1 \tag{20}$$

quantifies the delay caused by degradation periods in recovering the biomass from v_0 to v_1, with respect to the case when no disturbances occur. r is equal to zero when $\bar{T}(v_0, v_1) = \hat{T}(v_0, v_1)$ and becomes progressively larger if the difference between $\bar{T}(v_0, v_1)$ and $\hat{T}(v_0, v_1)$ increases.

3. Results

3.1. Preliminary Aspects

Typical hydrological and biomorphological characteristics were considered to explore the recovery dynamics of vegetation. To this aim, the benchmark set of parameters $\{C_h, \tau, k, a, \delta_{opt}\}_B = \{0.5, 0.01, 5, 0.5, 0.5\}$ was adopted. Figure 3a reports the trends of v_0 (the fifth percentile of biomass) and v_1 (the mean value) along the river transect. The transverse coordinate was made dimensionless so that $x = \eta$. Figures 3b–3d show the corresponding pdfs of vegetation biomass at three different locations along the transect, while Figures 3e–3g report the related enlarged views. We evaluated the difference ($v_1 - v_0$) as a useful metric of the flood-induced variability of biomass.

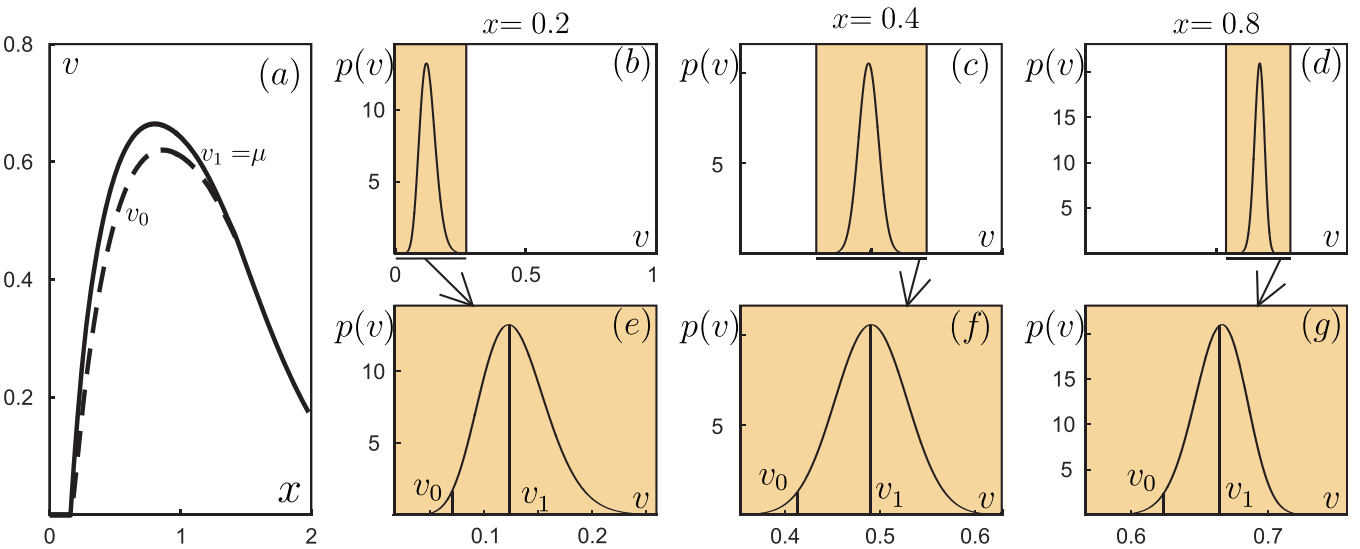

Figure 3. (a) Plot-specific mean value of biomass (v_1, continuous line) and fifth percentile of biomass (v_0, dashed line). (b–d) Plot-specific pdfs of biomass. (e–g) Enlarged views of the pdfs in Figures 3b–3d. Parameters are $\{C_h, \tau, k, a, \delta_{opt}\}_B = \{0.5, 0.01, 5, 0.5, 0.5\}$.

At a location relatively close to the river ($x = 0.2$), banks are almost bare ($v_0 \sim 0$), after hydrological events unfavorable to vegetation. Banks are weakly vegetated, on average ($v_1 \sim 0.15$). In plots with higher elevation ($x = 0.4$), v_0 and v_1 increase. As flooding conditions are not particularly severe, the banks are well vegetated on average, and also after unfavorable hydrological events.

At high elevation ($x = 0.8$) inundations are rare and weak. The plot is always well vegetated, and $p(v)$ is markedly peaked around its mean value v_1. Finally, far from the river ($x > 1$), the plot elevation becomes a limiting factor for tapping the phreatic surface. The vegetation suffers and its biomass decreases. By contrast, the effect of inundations is marginal and $(v_1 - v_0)$ tends to zero when $x \gg 1$.

3.2. Behavior of the Recovery Time

Let us first consider the recovery time in undisturbed conditions, $\hat{T}$, reported in Figure 4a. It spans a narrow range of values ($0.2 < \hat{T} < 0.5$), it is a nonlinear function of x and has a minimum at $x_{\min} = 0.5$. According to equation (19), $\hat{T}(x)$ is a decreasing function of the mean carrying capacity, β, which in turns depends on

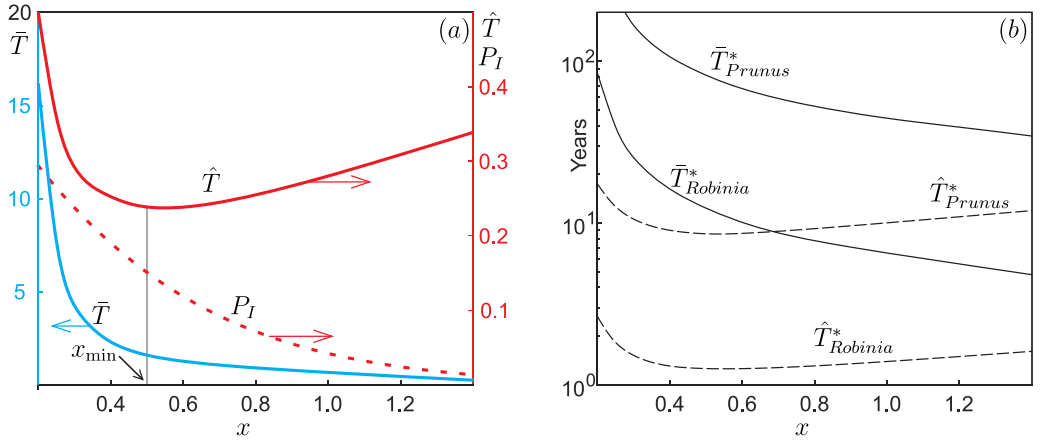

Figure 4. (a) Blue line and vertical axis on the left: dimensionless recovery time, $\bar{T}(v_0, v_1)$. Red line and vertical axis on the right: dimensionless recovery time in undisturbed conditions, $\hat{T}(v_0, v_1)$. Red dotted line and vertical axis on the right: probability of being flooded, P_I. $x_{\min}$ is the location in which $\hat{T}$ is minimum. v_0 (v_1) is the plot-specific fifth percentile (mean value) of biomass. (b) Dimensional recovery time, $\bar{T}^*(v_0, v_1)$, and recovery time in undisturbed conditions, $\hat{T}^*(v_0, v_1)$, for *Robinia pseudoacacia* ($\alpha_2 = 58 \times 10^{-5}$ day^{-1}) and *Prunus serotina* ($\alpha_2 = 7.8 \times 10^{-5}$ day^{-1}). In both panels, hydrological and biomorphological parameters are $\{C_h, \tau, k, a, \delta_{opt}\}_B = \{0.5, 0.01, 5, 0.5, 0.5\}$.

the depth of the water table, δ_{opt} (see equation (4)). The quantity $\hat{T}$ is therefore small as long as δ is close to the optimal depth (here set to 0.5). In the present dimensionless notation, $h = 0$ corresponds to the mean water stage, so $\bar{\delta}(x) = \eta = x$. It follows that (i) at $x < 0.5$, $\bar{\delta} < \delta_{opt}$ and root anoxia tends to slow down the vegetation growth; (ii) at $x = 0.5$, vegetation grows at optimal conditions, so $\hat{T}(x)$ reaches its minimum; and (iii) at $x > 0.5$, the water table is too deep and a weak capillary fringe hampers the optimal vegetation growth. Accordingly, when the water supply is the only limiting factor, the position $x = x_{\min}$ provides the optimal condition for growth. However, two other mechanisms also affect the behavior of $\hat{T}(x)$. The first mechanism is the dependency of the vegetation growth rate on the current biomass through equation (2b): the growth rate is small when v is close to zero or when it approaches the local carrying capacity, while it is maximum at intermediate values. In this last case, $\hat{T}(x)$ is minimum. The plot dependency of the difference between the fifth percentile of biomass and the mean biomass is responsible for the asymmetry of $\hat{T}(x)$ with respect to $x_{\min}$ ($v_1 - v_0$, in fact, varies from plot to plot). It follows that at high x the undisturbed recovery process is faster than at low x, because the difference between the initial v_0 and final v_1 biomass is lower.

Consider now the recovery time in stochastically disturbed conditions. Differently from $\hat{T}(x)$, $\bar{T}(x)$ exhibits high spatial gradients, variations of more than 1 order of magnitude, and a monotonic behavior. It is high close to the river but it decreases sharply moving away from the watercourse. All the processes that influence $\hat{T}$ affect $\bar{T}$ in a similar way. However, when stochasticity is considered, the plot-specific probability of being flooded, P_I, is the key factor in setting the value of $\bar{T}(x)$. It reads $P_I = 1 - \{\Gamma[\lambda] - \Gamma[\lambda, (1+x)\lambda]\}\Gamma[\lambda]$ and spans a wide range of values (Figure 4a, dotted curve). Close to the river, the probability of being flooded is high ($P_I = 0.3$). As the plot is inundated 30% of the time, floods damage the vegetation often. For low values of x, it is therefore very likely that while the biomass is recovering from v_0, a new flood may induce new damage before v_2 is reached. As a result, $\bar{T}$ is high. Far from the river, the probability of biomass to be damaged during the recovery decreases, so $\bar{T}$ is low. To check the soundness of Sancho's theory, and the validity of the assumption introduced (in particular, the use of α and β in place of the functions α_1 and V_{cc}), we have evaluated the recovery times of vegetation biomass by numerical integration of the complete model (2). Our results showed that recovery times evaluated by (16) never deviate more that $\pm 15\%$ from the numerically evaluated recovery times.

In order to evaluate the magnitude of recovery times in real cases, two typical riparian species are considered: *Robinia pseudoacacia* and *Prunus serotina* (Figure 4b). The former species grows fast and reaches the maximum size in less than 30 years ($\alpha_2 = 5.8 \times 10^{-4}$ day^{-1}) [*Redei et al*., 2014]. In absence of floods, its recovery time, $\hat{T}^*$, is less than 2 years. When stochastic flooding is considered, the recovery time increases significantly: at low plots, it is very high ($\bar{T}^* = 70$ years at $x = 0.2$) while at the site of the optimal undisturbed growth ($x_{\min} = 0.5$) it is about 10 years, i.e., 1 order of magnitude larger than the undisturbed recovery time. Finally, at higher plots, the mean and undisturbed recovery times approach each other.

A similar behavior is observed for *P. serotina*, a slowly growing species that reaches the maximum biomass in 200 years in optimal conditions ($\alpha_2 = 7.8 \times 10^{-5}$ day^{-1}) [*Camporeale and Ridolfi*, 2006]. In absence of floods, it recovers in about 10–20 years, depending on its location along the transect. When floods are considered, $\bar{T}^* > 200$ years at $x = 0.2$, while it is close to 80 years at $x_{\min} = 0.5$. It follows that, near the river, considerable time is necessary before the average biomass, $v = \mu$, is restored.

3.3. Sensitivity Analysis

According to the behavior of the curves $\hat{T}(x)$ and $\bar{T}(x)$ reported in Figure 4a, the metric r (defined in equation (20)) is very high at low x and it decreases with the plot elevation. To understand this behavior better, we performed a sensitivity analysis of r (see Figure 5) on the governing hydrological and biological parameters: the coefficient of variation, C_h; the vegetation sensitivity to floods, k; the time of correlation of the river water stage, τ; and the dependence of vegetation to the departure of the phreatic surface from its optimal position, a. This was done by changing one parameter at time from the benchmark set. When a model parameter was changed, the thresholds v_0 and v_1 changed as well. We refer to the panels on the right of Figure 5 for a qualitative explanation of the mechanisms involved. The upper half of each panel reports the temporal series of the water depth, $h - \eta$, in a given plot: $h - \eta > 0$ (<0) means inundation (exposure). The lower half of the panels reports the corresponding qualitative evolution of the biomass from v_0 up to the threshold v_1.

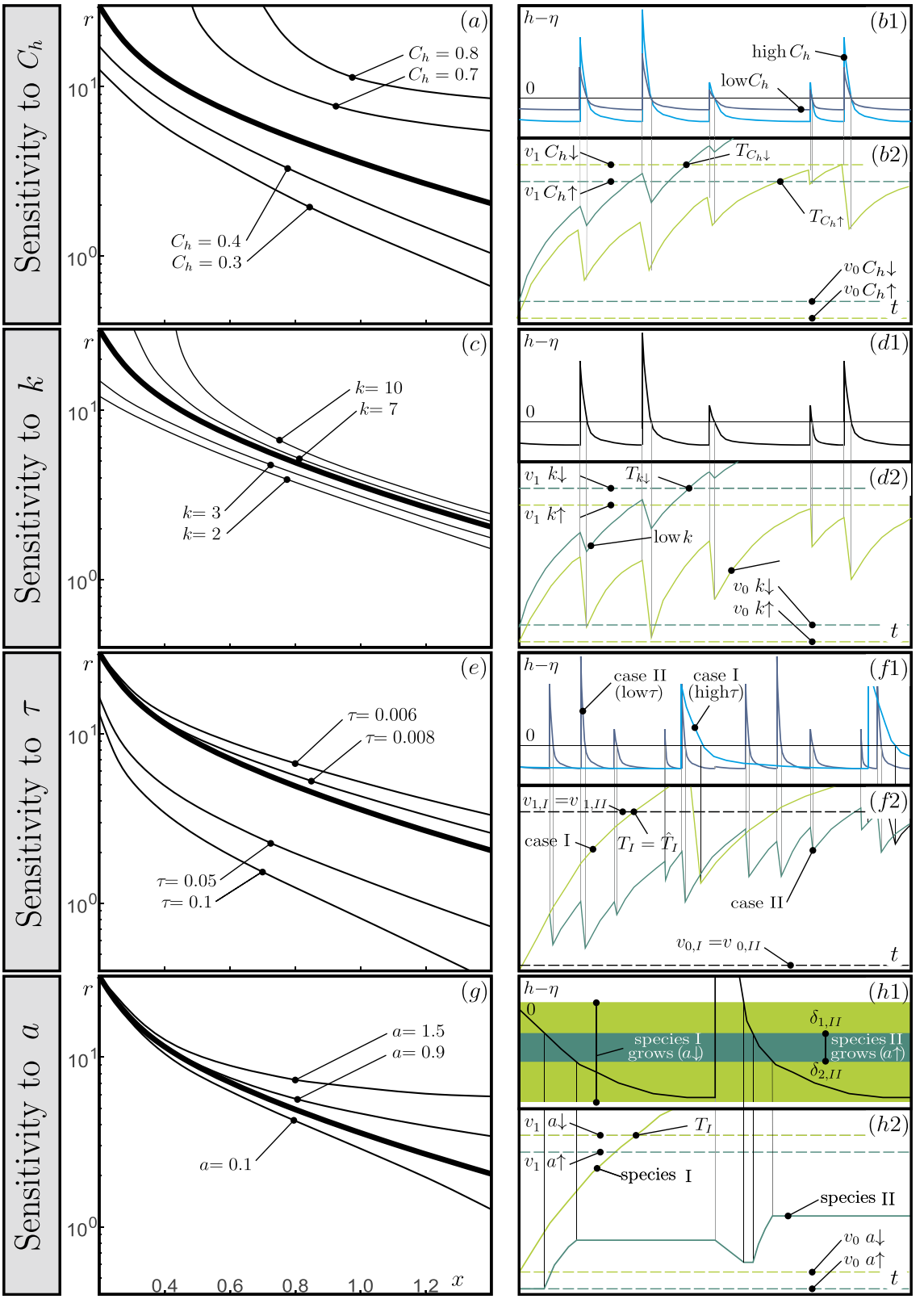

Figure 5. (left) Sensitivity analysis on r of the main modeling parameters. Only one parameter at time is changed with respect to the benchmark set $\{C_h, \tau, k, a, \delta_{opt}\}_B = \{0.5, 0.01, 5, 0.5, 0.5\}$. The black thick line reports r evaluated with the benchmark set. (right) Schematic explanation of the mechanisms behind the sensitivity of r on each parameter.

The coefficient of variation of the water stage affects r to a great extent, throughout the river transect (Figure 5a). In order to understand the reported behavior, Figure 5b1 shows two qualitative temporal series of the water stage, with low (dark blue) and high (light blue) values of C_h, respectively. In both series, the same mean value of $h-\eta$ and inundation times are adopted. In the first case (low C_h, dark green curve), the biomass grows undisturbed from v_0 until the occurrence of the first inundation and, since $h-\eta$ is small, the biomass lost is low (see equation (3)). After this loss of biomass, the vegetation starts to grow again and, after a sequence of a small number of growth and decline phases, the plot-specific mean biomass, $v=v_1=\mu$, is reached (see Figure 5b2). In the second case (high C_h, light green curve), the biomass lost during the first inundation phase is high. A large fraction of the recovered biomass is destroyed and a sequence of many growth/decrease phases is necessary to recover the plot-specific mean biomass. This behavior explains why recovery times increase with C_h. Moreover, as the increment of C_h implies an increment of P_I in any plot, this effect holds along the whole transect.

Figure 5c reports the impact of the vegetation sensitivity to floods, k. It is evident that the significant response is strongly plot dependent, as r spans 2 orders of magnitude along the transect. Figure 5d2 reports the response of two vegetation types characterized by a low (dark green line) and high (light green line) value of the parameter k, to the same water stage time series (Figure 5d1). Let us repeat the rationale applied in the previous paragraph regarding the impact of C_h. When the flood tolerance is high (i.e., low k) the vegetation that is lost during a flood is small, and the vegetation recovers very quickly. On the contrary, for high sensitivity to floods (high k), the recovery time is longer. In fact, a significant amount of vegetation biomass is lost during any flood. Since the inundation probability decreases with the elevation, an increment of k has a detrimental effect, especially in low plots.

Figure 5e describes the role of the correlation time τ. Basically, the curve $r(x)$ moves downward when τ increases and goes to zero at large x (that means $\bar{T} \simeq \hat{T}$). Again, two river stage time series have been considered in Figure 5f1, corresponding to high (case I, light blue) and small (case II, dark blue) correlation times, respectively. Alterations of the correlation scale, τ, mainly affect the water stage decay law [*Ridolfi et al.*, 2011]. We also assume that the two stage series have the same mean value and coefficient of variation. Finally, we set $\tau_{II} < \hat{T} < \tau_I$, with $\hat{T}=\hat{T}_I=\hat{T}_{II}$ (i.e., in both cases vegetation has the same undisturbed recovery time). At high correlation times (case I, light green), the biomass grows undisturbed from v_0 and recovers the mean biomass v_1 before the occurrence of the first inundation. At the same time, the long duration of the flood induces a significant biomass loss. When the time correlation is small (case II, dark green), short growth periods are frequently followed by quick floods, before the mean biomass v_1 is recovered. This mechanism is effective throughout the transect.

The role of the vegetation efficiency in tapping water from the aquifer is reported in Figure 5g. A significant change in r with a for $x \gtrsim 0.6$ is evident. Figure 5h1 shows a hypothetical temporal series of the phreatic surface. Two species are considered. Species I can tap the groundwater in a wide range of depth (low a, light green zone). Species II taps the groundwater in the narrow range of depth $[\delta_{1,II}, \delta_{2,II}]$ (high a, dark green zone). Consider first the biomass evolution of species I (Figure 5h2, dark green curve). The depth of the phreatic surface always lies within the range that allows growth and v grows undisturbed from v_0 to v_1. Consider now the biomass evolution of species II (light green curve). While the water level is in the range $[0, \delta_{1,II}]$, the phreatic surface is too shallow, and species II does not grow. When $h-\eta \in [\delta_{1,II}, \delta_{2,II}]$, the phreatic surface is at an appropriate depth, and species II grows. When $h-\eta$ is below $\delta_{2,II}$ the phreatic surface is too deep, and the biomass growth is halted. As a result of the low water tapping efficiency, a low net biomass increment is attained between consecutive floods, and the biomass recovery is slow.

In Table 1, the sensitivity of r on the model parameter is systematically evaluated in three plots. To this aim, we first evaluate the plot-specific r_B, i.e., r evaluated with benchmark parameters (second line of Table 1). Then, one parameter at time is changed of -20%, -10%, $+10\%$, and $+20\%$ with respect to its benchmark value, and r is evaluated again. Finally, the ratio r/r_B is computed to measure the departure of r from r_B. All the typical behaviors previously described are confirmed, and, in particular: (i) the role of the coefficient of variation is predominant at any plot, and changes of C_h of $\pm 20\%$ can induce variation of r of more than 50%; (ii) the variation of the correlation time affects everywhere r/r_B, but alterations of τ up to $\pm 20\%$ change r no more than 13%; (iii) the vegetation sensitivity to floods matters (is not significant) at low (high) plots, where variations of r of $\sim 10\%$ ($\sim 1\%$) are attained by changing k of $\pm 20\%$; (iv) the efficiency in tapping

Table 1. Ratio r/r_B at Different Plots (Columns) and for Alteration of One Parameter at Time (Rows)[a]

	$x = 0.4$ ($r_B = 11.29$)				$x = 0.8$ ($r_B = 5.40$)				$x = 1.2$ ($r_B = 3.32$)			
	−20%	−10%	+10%	+20%	−20%	−10%	+10%	+20%	−20%	−10%	+10%	+20%
C_h	0.78	0.87	1.18	1.52	0.74	0.87	1.14	1.29	–	–	1.20	1.41
τ	1.12	1.06	0.95	0.91	1.13	1.06	0.95	0.90	–	1.06	0.94	0.89
K	0.90	0.95	1.06	1.13	0.97	0.99	1.02	1.03	0.99	1.00	1.01	1.02
A	0.99	0.99	1.00	1.01	0.97	0.98	1.02	1.04	0.92	0.96	1.04	1.09

[a]Each parameter is altered of −20%, −10%, +10%, and +20%, with respect to its benchmark value. The benchmark set is $\{C_h, \tau, k, a, \delta_{opt}\}_B = \{0.5, 0.01, 5, 0.5, 0.5\}$. Notice that in some cases (denoted by "–") the parameter set is unsuitable for vegetation growth, and the recovery time has not been evaluated.

water is important (plays no role) at high (low) plots, where changes of r up to ∼10% (less than 1%) are attained with changes of a of ±20%.

3.4. Impact of River Flow Alterations

River flow alterations are widespread, have different causes (climate change, hydroplants, river regulations, irrigation, etc.), and can affect the riparian vegetation in several ways. Typical features are the shifting of the vegetated front, the widening-narrowing of the river channel, the establishment of vegetation on river islands, and the proliferation of exotic species to the detriment of the indigenous vegetation [*Richardson et al.*, 2007; *Tealdi et al.*, 2011; *Doulatyari et al.*, 2014]. In this picture, the previous analytical results allow the impact of river flow alterations on the vegetation recovery times to be investigated in detail.

The most striking and investigated alteration is a reduction of the mean flow rate. In addition, the change in the probabilistic structure of the river flow time series (summarized by the coefficient of variation and the autocorrelation time) can induce detrimental effects on the vegetation dynamics [*Shafroth et al.*, 2002; *Tealdi et al.*, 2011]. Since the impacts of the latter modification are subtle and counter intuitive, we will focus on the changes of C_h and τ, while maintaining the mean flow unaltered.

Figure 6a reports the combined effect of changes of C_h and τ on the metric r. It grows when C_h increases and reduces if τ increases. It is worth noticing that, up to $C_h \simeq 0.6$ (in the benchmark case considered), the increment of r can be balanced by an increment of τ. For example, let us consider a river stage regime characterized by $\{\tau, C_h\} = \{0.01, 0.4\}$ (point A in Figure 6). If the coefficient of variation of the stage is moved to $C_h = 0.6$ (point B), r doubles from 6 to 12. This impact could be balanced by increasing τ. In fact, at point C ($\{\tau, C_h\} = \{0.04, 0.6\}$), the value $r = 6$ is restored. Differently, if C_h rises to $C_h = 0.67$ (point D, where $r = 18$), no increments of τ can reduce r back to 6. It follows that the flow alterations that induce high values of C_h ($>$0.6 in this specific example) make a quick recover impossible and not remediable by changes in τ. Therefore, there is a threshold of C_h beyond which the efficiency of an increment of τ in reducing r drops. This threshold depends on the probability of being flooded, P_f, and it is therefore plot dependent (see Figure 4a). By increasing (reducing) the plot elevation, this threshold of C_h increases (reduces).

The chart reported in Figure 6a can be adopted for assessing the impact of some typical hydraulic alterations. Consider first hydropeaking, i.e., the sudden release of a large flow in the river (typically from a hydroelectric power station). From a hydrological viewpoint, hydropeaking reduces the correlation time and increases the coefficient of variation of the stage time series, with respect to natural conditions. For a regime altered by hydropeaking, the set of parameters $\{\tau, C_h\}$ lies in the upper left corner of the plot, where r is high and vegetation recover is very long. Previous studies [*Camporeale and Ridolfi*, 2006] demonstrated also that the higher C_h, the lower the mean plot biomass. C_h has therefore a twofold detrimental effect. It follows that very long time is required to grow little biomass in banks of hydropeaking affected rivers. As a result, we expect that these banks are generally weakly vegetated.

Consider now dams used for the management of flooding and for the flow regulation. During a flood, a dam retains most of the river flow rate in the reservoir, allowing for a downstream flow rate that is not hazardous for human infrastructures. This smoothing out of floods by the dam is defined *flood lamination*. Notice that the dam can laminate a flood as long as there is space in the reservoir to accommodate the incoming water, but when the reservoir is full, the whole river flow rate is convected downstream. As a result of this flow regulation, the set $\{\tau, C_h\}$ falls in the lower right corner of the plot, where r is very low,

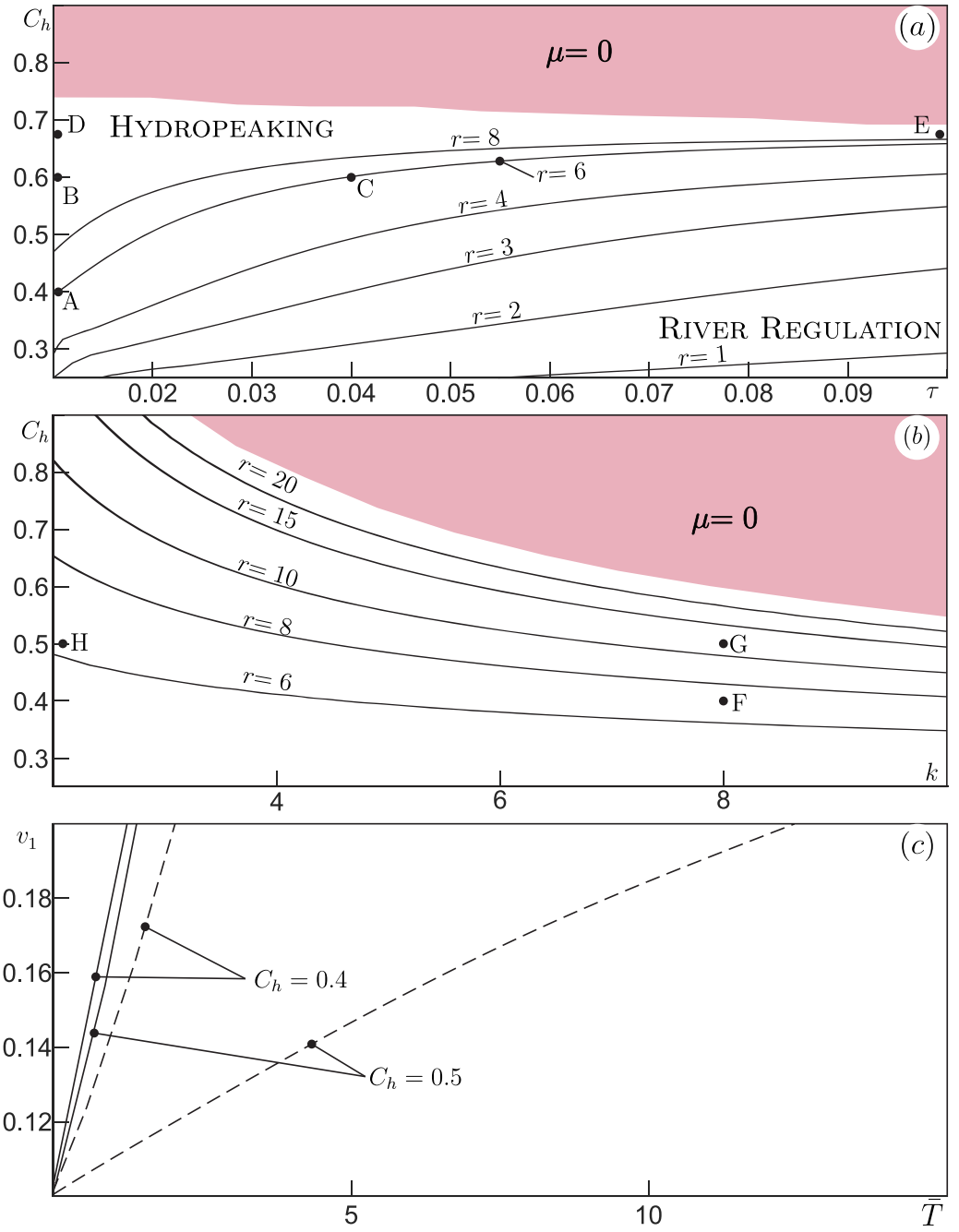

Figure 6. (a, b) Behavior of the metric r in the planes $\{\tau, C_h\}$ and $\{k, C_h\}$, respectively. The pink region corresponds to conditions unsuitable to vegetation growth. Other parameters correspond to the benchmark set $\{C_h, \tau, k, a, \delta_{opt}\}_B = \{0.5, 0.01, 5, 0.5, 0.5\}$. (c) Relation between the threshold biomass v_1 and the mean time $\bar{T}$ required to reach v_1 for two values of C_h. The continuous and dotted lines identify the flood-tolerant and flood-sensitive species, respectively. All panels refer to $x = 0.5$.

i.e., the recovery of vegetation is fast. This may be related to some previous theoretical [*Camporeale and Ridolfi*, 2006; *Tealdi et al*., 2011] and field [*Shafroth et al*., 2002] studies. In regulated rivers where the detrimental effect of floods is removed, vegetation extends its coverage; increases its biomass; and colonizes sites very close to the stream. This kind of channel narrowing can be potentially dangerous for the downstream infrastructures and human activities. Consider for instance a dam that cannot laminate very intense or long floods. If an inundation of this type occurs, vegetation is submerged. As a result, the water stage grows significantly, with respect to the nonvegetated case (in fact, vegetation increases bed roughness), and can induce the overtopping of banks. Moreover, the vegetal biomass can be eradicated and

transported downstream. This large amount of woody debris can be hazardous for the stability of river infrastructure.

In order to explore the biological implications related to changes of the coefficient of variation of the river stage, Figure 6b shows the combined effect of C_h and k on r. The key feature is that an increment of C_h induces a delay of the vegetation recovery. For instance, consider a flood-sensitive species ($k = 8$) that grows along a river with $C_h = 0.4$ (point F). If C_h rises to 0.5, the recovery time grows (i.e., r moves from 6 to >10, see point G). In this case, a more flood-resistant vegetation (e.g., $k = 2$, point H) exhibits a fast recovery time ($r \sim 6$).

The impact of changes of the river flow probabilistic structure on the competition between different vegetation species is a key issue which deserves further attention. To this aim, recall that $\bar{T}(v_0, v_1)$ is the mean time required by biomass to grow from v_0 to v_1. By evaluating $\bar{T}(v_0, v_1)$ for different values of v_1, one can plot a curve in the plane $\{\bar{T}, v_1\}$. This curve provides the biomass v_1 typically attained after a time $\bar{T}$, starting from the initial biomass v_0. This curve is reported in Figure 6c for four emblematic sets of parameters $\{k, C_h\}$, with $v_0 = 0.1$ and $0.1 < v_1 < 0.2$. Two species of plants are considered: a flood-tolerant species I ($k_I = 2$), and a flood-sensitive species II ($k_{II} = 8$). In order to focus on the impact of flood-induced disturbances on the species coexistence, any other interspecies competition/cooperation mechanism is disregarded.

If an original river flow sequence with $C_h = 0.4$ is considered, both species exhibit a fast recovery dynamics with comparable timescales: at $\bar{T} \simeq 2$, one observes $v_{I,2} \simeq v_{II,2} \simeq 0.2$. If the coefficient of variation of the water stage is then increased to $C_h = 0.5$ (dashed lines), the recovery time of the flood-resistant species changes very little. By contrast, the recovery time of the flood-sensitive species significantly increases. Therefore, a mild increment of the river stage variability changes dramatically the recovery dynamics of a species. For a long period ($\bar{T} \simeq 10$), the biomass of the species I is much larger than the biomass of the species II. This mechanism, combined with the effect of other interspecies competitions dynamics, can lead to the dominance of species I to the detriment of species II. A similar qualitative scenario emerges if a change in the river stage correlation time is considered. The analysis of the recovery times can be a valuable tool to investigate how the species distribution along the riparian transect is affected by alterations of the probabilistic characteristics of river flow time series. In our analysis, we found that even mild alterations can have significant effects on the temporal dynamics of the recovery process.

3.5. Spatial Dynamics of the Vegetation Recovery

Analytical results obtained in the previous sections allow the spatial behavior of the recovery dynamics along the transect to be investigated. To this aim, let us assume that riparian vegetation has been damaged by a strong flood event and biomass has been reduced to a low value, v_0, at all plots. Without any loss of generality, we set $v_0 = 0.01\mu$, where μ is the plot-specific averaged value of the biomass distribution, $p(v)$. From this destructive event, the recovery phase begins. In the previous sections, the parameter $\bar{T}(v_0, v_1)$ has been used to obtain the average time necessary to recover a given state v_1 starting from $v = v_0$. We now consider different values of $\bar{T}$ and obtain the corresponding values of v_1, namely the typical biomass reached after a time $\bar{T}$ has passed. $\bar{T}(v_0, v_1)$ depends on a number of plot-specific factors. It follows that different values of v_1 are expected along the transect, for the same given $\bar{T}$. This concept is reported in Figure 7a. The lower thick red line represents the starting biomass v_0 along the transect, while the thin lines describe the biomass distribution for given values of $\bar{T}$. Biomass recovery occurs with different time scales in different plots and, in particular, more rapid recovery is observed away from the river, where plots have a higher elevation. Note that the curves saturate to $v = v_1 = \mu$ (thick blue curve, the conventional ending point of the recovery phase, according to the previous sections). For better understanding this point, let us consider the case $\bar{T} = 15$. The recovery from v_0 to $v = \mu(x)$ is complete at $x \simeq 0.42$ (point A), while at $x \sim 0.22$ (point B), the recovery is still very weak.

Figure 7a shows that (i) the recovery process is highly heterogeneous in space and (ii) the spatial dynamics of vegetation recovery resemble a wave that propagates toward the river and progressively saturates to the local value of v_1. This interpretation leads to the definition of a typical wave celerity. To this aim, consider the plot closest to the river where the recovery is complete (e.g., point A for $\bar{T} = 15$). This point can be assumed as the front of the recovery wave, and its position is x_{rf}, where subscript "rf" refers to "recovery front." In Figure 7a, the position of the front at $\bar{T} = 15$, 20, and 30 is marked. Accordingly, the displacement velocity of x_{rf} identifies the celerity of the recovery wave, namely

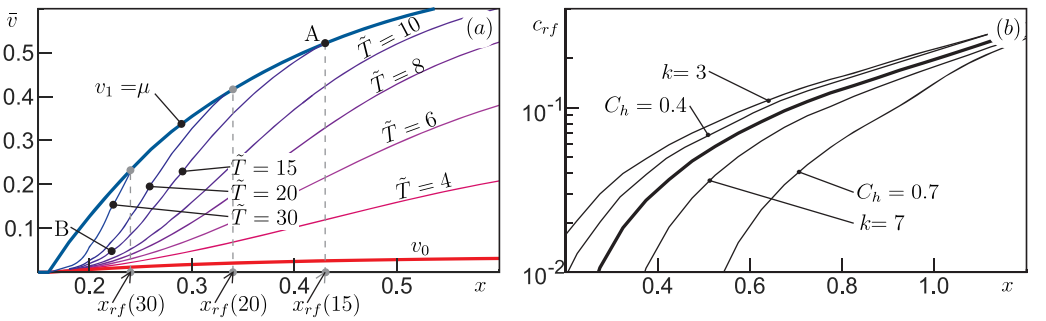

Figure 7. (a) Wave-like dynamics of vegetation recovery along the transect. Thick lines show the biomass behavior at the start of the recovery process ($v_0 = 0.01\mu$, lower red line), and at the end ($v_1 = \mu$, upper blue line). Thin lines report the typical biomass reached at different times $\tilde{T}$. (b) Behavior of wavefront celerity, c_{rf}, along the transect. Thick line refers to the benchmark condition $\{C_h, \tau, k, a, \delta_{opt}\}_B = \{0.5, 0.01, 5, 0.5, 0.5\}$ while thin lines show the sensitivity to some modeling parameters.

$$c_{rf} = \frac{\partial x_{rf}(\tilde{T})}{\partial \tilde{T}}. \tag{21}$$

The behavior of c_{rf} along the transect is shown in Figure 7b, where its sensitivity to C_h and k is also explored. The key feature is the progressive and more-than-linear slowing of the recovery front as the river is approached. As expected, C_h impacts the celerity to a great extent. In particular, c_{rf} decreases when the river stage time series is more fluctuating. Finally, the recovery is delayed for high values of k, that is, the more flood-tolerant the vegetation, the higher the celerity of the recovery front.

4. Conclusions

In this study, the recovery dynamics of riparian vegetation have been analyzed. To this aim, we have adopted the ecohydrological stochastic approach by *Camporeale and Ridolfi* [2006], and the plot-dependent recovery times have been obtained by using the theory developed by *Sancho* [1985] for the evaluation of the mean first passage time in dynamical systems driven by dichotomous noise.

The main result is that the average recovery time, $\bar{T}$, is much longer (up to 1 order of magnitude) than the recovery time in undisturbed conditions, $\hat{T}$. The delay in the recovery process is due to the random fluctuations of the river stage that cause alternate phases of vegetation growth and degradation rather than a monotonic growth of biomass. The maximum impact of river-induced disturbances is close to the stream, where inundations with the highest duration, magnitude, and frequency occur. Our results show that a long time is required to obtain a net increment of biomass in plots close to the river and, thus, long periods of observation are necessary to acquire a realistic picture of the biomass variability. A single observation at a given time corresponds to very different phases in the recovery of each plot. This can be seen from the wave-like behavior of the recovery dynamics along the transect.

The sensitivity analysis has revealed that recovery times are heavily influenced by the hydrological regime of the river and by the sensitivity of vegetation to floods. More in details, the autocorrelation timescale of the river water stage plays a key role in determining how fast the biomass evolves between different thresholds.

The impact of hydrological regime alterations has been discussed from a viewpoint of recovery dynamics. Since modifications of C_h or τ have a remarkable influence on vegetation, it is possible to smooth out—within limits—the effect of man-induced river flow alterations on the recovery times by a suitable modification of these two parameters. This approach may help to plan river flow management strategies for preserving the vegetation biodiversity and reducing the anthropic impact in dammed and regulated rivers. On the contrary, we have demonstrated how also mild unbalanced alterations of the probabilistic structure of the river flows can induce dramatic effects on recovery times, contributing in biodiversity losses and invasions of exotic species.

Recent studies elucidated the importance of the river-induced randomness in shaping riparian vegetation dynamics. In these investigations, the steady state pdf of biomass was used as an interpretative metamathematical tool. In the present work, we have adopted a different perspective by exploring the temporal structure of plot-dependent biomass time series. Our findings confirm and underline the crucial role played by noise, to the point that any action on the fluvial environment (e.g., restoration projects, water diversion, and river regulation) should consider randomness as a fundamental ingredient to forecast consequences.

Appendix A: Expression of $p(v)$, α, β, k_E, and k_I

The average rate of vegetation degradation and the mean carrying capacity read, respectively,

$$\alpha = \frac{k\lambda^{\lambda-1}e^{-\lambda(\eta+1)}(\eta+1)^{\lambda}}{\Gamma[\lambda,(\eta+1)\lambda]} - k\eta,$$

$$\beta = \frac{\lambda[a(\eta-\delta_{opt})-1](\Gamma[\lambda,(\delta_2+1)\lambda]-\Gamma[\lambda,(\delta_1+1)\lambda]) + a\lambda^{\lambda}\left[e^{-\lambda(\delta_1+1)}(\delta_1+1)^{\lambda}-e^{-\lambda(\delta_2+1)}(\delta_2+1)^{\lambda}\right]}{\lambda(\Gamma[\lambda]-\Gamma[\lambda,(\eta+1)\lambda])}.$$

The switching rate of the exposure conditions is equal to

$$k_E = \frac{\lambda^{\lambda}e^{-\lambda(\eta+1)}(\eta+1)^{\lambda}}{\tau\Gamma[\lambda]-\tau\Gamma[\lambda,(\eta+1)\lambda]},$$

while the switching rate of the inundated conditions is given by

$$k_I = \frac{e^{-\lambda(\eta+1)}}{\tau E_{1-\lambda}[(\eta+1)\lambda]},$$

where $E_{1-\lambda}[\cdot]$ is the exponential integral function [*Abramowitz and Stegun*, 1964].

Acknowledgment
This work presents a theoretical study and no measured data were used.

References

Abramowitz, M., and I. Stegun (1964), *Handbook of Mathematical Functions: With Formulas, Graphs, and Mathematical Tables*, Dover, N. Y.
Bertoldi, W., A. Siviglia, S. Tettamanti, M. Toffolon, D. Vetsch, and S. Francalanci (2014), Modeling vegetation controls on fluvial morphological trajectories, *Geophys. Res. Lett.*, *41*, 7167–7175, doi:10.1002/2014GL061666.
Beschta, R. L., and W. J. Ripple (2006), River channel dynamics following extirpation of wolves in northwestern Yellowstone National Park, USA, *Earth Surf. Processes Landforms*, *31*(12), 1525–1539.
Blanchard, R., and P. M. Holmes (2008), Riparian vegetation recovery after invasive alien tree clearance in the Fynbos Biome, *S. Afr. J. Bot.*, *74*(3), 421–431.
Camporeale, C., and L. Ridolfi (2006), Riparian vegetation distribution induced by river flow variability: A stochastic approach, *Water Resour. Res.*, *42*, W10415, doi:10.1029/2006WR004933.
Camporeale, C., and L. Ridolfi (2007), Noise-induced phenomena in riparian vegetation dynamics, *Geophys. Res. Lett.*, *34*, L18406, doi:10.1029/2007GL030899.
Camporeale, C., E. Perucca, L. Ridolfi, and A. M. Gurnell (2013), Modeling the interactions between river morphodynamics and riparian vegetation, *Rev. Geophys.*, *51*, 379–414, doi:10.1002/rog.20014.
Craig, L. S., et al. (2008), Stream restoration strategies for reducing river nitrogen loads, *Front. Ecol. Environ.*, *6*(10), 529–538.
Crosato, A., and M. S. Saleh (2011), Numerical study on the effects of floodplain vegetation on river planform style, *Earth Surf. Processes Landforms*, *36*(6), 711–720.
Crouzy, B., F. Brenbold, P. D'Odorico, and P. Perona (2015), Ecomorphodynamic approaches to river anabranching patterns, *Adv. Water Resour.*, doi:10.1016/j.advwatres.2015.07.011, in press.
Docker, B. B., and T. C. T. Hubble (2008), Quantifying root-reinforcement of river bank soils by four Australian tree species, *Geomorphology*, *100*(3–4), 401–418.
Doulatyari, B., S. Basso, M. Schirmer, and G. Botter (2014), River flow regimes and vegetation dynamics along a river transect, *Adv. Water Resour.*, *73*, 30–43.
Gibling, M. R., and N. S. Davies (2012), Palaeozoic landscapes shaped by plant evolution, *Nat. Geosci.*, *5*(2), 99–105.
Gurnell, A., D. C. Corenblit, D. Garca de Jaln, M. Gonzlez del Tnago, R. Grabowski, M. O'Hare, and M. H. Szewczyk (2015), A conceptual model of vegetation-hydrogeomorphology interactions within river corridors, *River Res. Appl.*, *32*, 142–163.
Hupp, C. R. (1988), Plant ecological aspects of flood geomorphology and paleoflood history, in *Flood Geomorphology*, edited by V. R. Baker, R. C. Koche, and P. C. Patton, pp. 335–356, John Wiley, Hoboken, N. J.
Kitahara, K., W. Horsthemke, R. Lefever, and Y. Inaba (1980), Phase-diagrams of noise induced transitions—Exact results for a class of external colored noise, *Prog. Theor. Phys.*, *64*(4), 1233–1247.
Kozlowski, T. (1984), Responses of woody plants to flooding, in *Flooding and Plant Growth, Physiol. Ecol.*, edited by T. Kozlowski, pp. 129–163, Academic, Orlando, Fla.
Kurokochi, H., K. Toyama, and T. Hogetsu (2010), Regeneration of *Robinia pseudoacacia* riparian forests after clear-cutting along the Chikumagawa River in Japan, *Plant Ecol.*, *210*(1), 31–41.
Laio, F., A. Porporato, L. Ridolfi, and I. Rodriguez-Iturbe (2001), Mean first passage times of processes driven by white shot noise, *Phys. Rev. E*, *63*, 036105.

Malanson, G. (1993), *Riparian Landscapes*, Cambridge Univ. Press, Cambridge.
Marshall, K. N., N. T. Hobbs, and D. J. Cooper (2013), Stream hydrology limits recovery of riparian ecosystems after wolf reintroduction, *Proc. R. Soc. B*, *280*(1756).
Muneepeerakul, R., A. Rinaldo, and I. Rodriguez-Iturbe (2007), Effects of river flow scaling properties on riparian width and vegetation biomass, *Water Resour. Res.*, *43*, W12406, doi:10.1029/2007WR006100.
Naiman, R., H. Décamps, and M. McClain (2005), *Riparia*, Elsevier, Burlington.
Naumburg, E., R. Mata-gonzalez, R. G. Hunter, T. Mclendon, and D. W. Martin (2005), Phreatophytic vegetation and groundwater fluctuations: A review of current research and application of ecosystem response modeling with an emphasis on great basin vegetation, *Environ. Manage.*, *35*(6), 726–740.
Nicholas, A. P., P. J. Ashworth, G. H. S. Smith, and S. D. Sandbach (2013), Numerical simulation of bar and island morphodynamics in anabranching megarivers, *J. Geophys. Res. Earth Surf.*, *118*, 2019–2044, doi:10.1002/jgrf.20132.
Osterkamp, W. R., and J. E. Costa (1987), Change accompanying an extraordinary flood on sandbed stream, in *Catastrophic Flooding*, edited by L. Mayer and D. Nash, pp. 201–224, Allen and Unwin, St. Leonards, N. S. W., Australia.
Redei, K., I. Csiha I, Z. Keserű, J. Rásó, Á. K. Végh, and B. Antal (2014), Growth and yield of black locust (*Robinia pseudoacacia* L.) stands in Nyirseg growing region (North-East Hungary), *South-East Eur. For.*, *5*(1), 13–22, doi:10.15177/seefor.14-04.
Richardson, D. M., P. M. Holmes, K. J. Esler, S. M. Galatowitsch, J. C. Stromberg, S. P. Kirkman, P. Pysek, and R. J. Hobbs (2007), Riparian vegetation: degradation, alien plant invasions, and restoration prospects, *Divers. Distrib.*, *13*(1), 126–139.
Ridolfi, L., P. D'Odorico, and F. Laio (2011), *Noise-Induced Phenomena in the Environmental Sciences*, Cambridge Univ. Press, Cambridge.
Sancho, J. (1985), External dichotomous noise—The problem of the mean 1st-passage time, *Phys. Rev. A*, *31*(5), 3523–3525.
Shafroth, P., J. Stromberg, and D. Patten (2002), Riparian vegetation response to altered disturbance and stress regimes, *Ecol. Appl.*, *12*(1), 107–123.
Singer, F., L. Mark, and R. Cates (1994), Ungulate herbivory of willows on Yellowstone northern winter range, *J. Range Manage.*, *47*(6), 435–443.
Smith, D. B., D. Finch, C. C. Gunning, R. Jemison, and J. Kelly (2009), Post-wildfire recovery of riparian vegetation during a period of water scarcity in the southwestern USA, *Fire Ecol.*, *5*(1), 38–55.
Srinivasan, V., and P. Kumar (2015), Emergent and divergent resilience behavior in catastrophic shift systems, *Ecol. Modell.*, *298*(SI), 87–105.
Surian, N., M. Barban, L. Ziliani, G. Monegato, W. Bertoldi, and F. Comiti (2015), Vegetation turnover in a braided river: Frequency and effectiveness of floods of different magnitude, *Earth Surf. Processes Landforms*, *40*(4), 542–558.
Tealdi, S., C. Camporeale, and L. Ridolfi (2011), Modeling the impact of river damming on riparian vegetation, *J. Hydrol.*, *396*(3–4), 302–312.
Tockner, K., F. Malard, and J. Ward (2000), An extension of the flood pulse concept, *Hydrol. Processes*, *14*(16–17), 2861–2883.
Tron, S., P. Perona, L. Gorla, M. Schwarz, F. Laio, and L. Ridolfi (2015), The signature of randomness in riparian plant root distributions, *Geophys. Res. Lett.*, *42*, 7098–7106, doi:10.1002/2015GL064857.
Vandenbroeck, C. (1983), On the relation between white shot noise, Gaussian white noise, and the dichotomic Markov process, *J. Stat. Phys.*, *31*(3), 467–483.
Vesipa, R., C. Camporeale, and L. Ridolfi (2015), Noise-driven cooperative dynamics between vegetation and topography in riparian zones, *Geophys. Res. Lett.*, *42*, 8021–8030, doi:10.1002/2015GL065688.
Ward, J., K. Tockner, P. Edwards, J. Kollmann, G. Bretschko, A. Gurnell, G. Petts, and B. Rossaro (1999), A reference river system for the Alps: The Fiume Tagliamento, *Regul. Rivers Res. Manage.*, *15*(1–3), 63–75.
Wu, W., F. Shields, S. Bennett, and S. Wang (2005), A depth-averaged two-dimensional model for flow, sediment transport, and bed topography in curved channels with riparian vegetation, *Water Resour. Res.*, *41*, W03015, doi:10.1029/2004WR003730.
Yanosky, T. M. (1980), Effects of flooding upon woody vegetation along parts of the Potamac River flood plain, *U.S. Geol. Surv. Prof. Pap.*, *1206*, 1–21.